JOURNAL OF MATERIALS SCIENCE 31 (1996) 5716–5722

Influence of residual stresses and interfacial shear strength on matrix properties in fibre-reinforced ceramic matrix composites

S. KUMARIA, R. N. SINGH
Department of Materials Science and Engineering, University of Cincinnati, Cincinnati, OH 45221, USA

Zircon matrix composites, uniaxially reinforced with a variety of SiC fibres were fabricated in order to create composites with different interfacial properties. Interfacial properties were varied by changing the nature of fibre coatings. The effect of changes in interfacial shear strength on important matrix properties, such as hardness and fracture toughness, was studied on a micro-scale using the microindentation technique. In addition, the relative orientation of the indented cracks with respect to the fibres was varied to investigate the existence of anisotropic behaviour of the matrix. The results indicated that the crack growth in the matrix was influenced by the presence of residual radial and axial stresses, such that relatively higher crack lengths were seen in certain directions in the matrix with respect to other directions. This asymmetric nature of the crack formation upon indentation was the reason for the observed anisotropic fracture toughness of the matrix. The residual stresses also led to anisotropic hardness and a critical load for crack initiation in the matrix.

1. Introduction

The fibre–matrix interfacial properties play a dominant role in controlling the mechanical response of composites, together with factors such as mechanical properties of the fibre and matrix, and the processing conditions. Optimization of the interfacial shear strength can lead to a considerable enhancement in toughness and strength of a composite [1–3]. These observations on improved mechanical response have, however, been made for properties of fibre-reinforced composites on a macro-scale and not on a micro-scale. An effective way to study the influence of interfacial properties on the mechanical response of composites on a micro-scale is to use the micro-indentation technique, which is now a readily accepted and implemented method to evaluate important physical properties such as fracture toughness and hardness of the monolithic ceramics [4–15]. In recent years, this method has also been used to investigate the existence of anisotropic mechanical behaviour in whisker-reinforced ceramic composites [16–18]. Wang *et al.* [19] have reported measurements of fracture toughness in a randomly oriented short-fibre ceramic composite. Powell *et al.* [20] have calculated the microhardness in a continuous fibre-reinforced ceramic composite, although a detailed quantitative analysis has not been performed.

In the present investigation, the technique of micro-indentation was used to study the influence of changes in interfacial shear strength on matrix properties on a micro-scale in continuous fibre-reinforced ceramic composites.

2. Experimental procedure

Monolithic zircon and zircon-matrix composites, uniaxially reinforced with silicon carbide fibres, were fabricated by the method described in Singh [21]. Interfacial properties were modified by using either the as-supplied silicon carbide fibres (Textron–SCS–6 and SCS–0) or coating them with a thin layer of boron nitride or carbon. The composite made by using the as-supplied SCS–6 fibres is designated UNC (uncoated) and that with the boron nitride coating, BN. The sample made by using as-supplied SCS–0 fibres is designated Si-R (silicon rich) and that made with SCS-0 fibres having a carbon-rich surface is designated C-R. The uncoated and boron nitride-coated samples created a weakly bonded interface, while the carbon-rich and silicon-rich fibres surfaces resulted in relatively stronger interfaces [22]. The interfacial shear strength in these composites decreased as BN < UNC < C-R < Si-R. A summary of composite characteristics and interfacial properties for these composites is given in Table I.

Specimens representing these four types of interfaces were polished in two different orientations. These orientations have been referred to as longitudinal (LN) and transverse (TR). A schematic drawing of the two orientations is given in Fig. 1. Polishing was done with diamond pastes of progressively increasing fineness leading to a final finish with a 1 μm size. This ensured that the surface damage produced during grinding and rough polishing stages was minimized so that the final sample surface was relatively free of polishing-induced stresses prior to the indentation studies [6].

0022–2461

TABLE I Interfacial properties as calculated by the shear-lag model [22]

Composite (coating)	τ_d[a] (MPa)	σ_N[b] (MPa)	μ[c]	τ_f[d] (MPa)
BN (boron nitride)	8.80	31.67	0.21	6.63
UNC (uncoated)	13.35	31.63	0.23	7.43
C-R (carbon-rich)	40.35	14.88	0.95	14.16
Si-R (silicon-rich)	$\approx$100	–	–	–

[a] Interface debond shear strength.
[b] Residual normal stress.
[c] Coefficient of friction.
[d] Frictional shear strength.

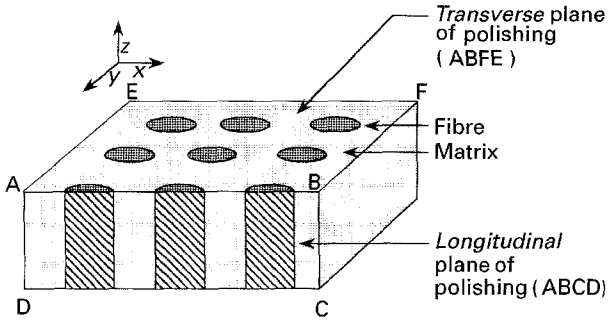

Figure 1 Schematic illustration of a composite showing two planes of polishing for the different samples.

A Vickers pyramid micro-indentor made of diamond was used to measure the hardness, fracture toughness, and crack initiation load for both the monolithic zircon and fibre-reinforced composites. Samples in the longitudinal and transverse orientations were indented to obtain matrix properties on a micro-scale using the following approaches.

2.1. Hardness (H)

A load of 0.7 kg was used to measure the Vickers hardness of all the samples. This load was chosen because it created indentation impressions which were large enough to be measured accurately. Vickers hardness was calculated using the relation [23]

$$H = 1.854P/L^2 \quad (1)$$

where P is the indentation load (kg), and L is the average length of the indentation diagonals (mm). A set of 10 indentations was made on each sample to calculate the average hardness.

2.2. Fracture toughness, K_{Ic}

Initially, trial indentations were made in the load range of 1–4 kg for the monolithic and composite samples to find a suitable load for fracture toughness measurements. A distance of more than four times the approximate crack length was maintained between the centres of any two adjacent indentations to ensure that the cracks from one indentation did not interact with those of the other. Also, the crack lengths were measured immediately after an indentation to avoid any post-indentation crack growth [6]. A load of 2.5 kg was chosen to make indentations for fracture toughness measurements, because this load produced consistent and well-formed cracks with a symmetrical pattern. Indentations were made in the matrix at the mid-point between two fibres in the longitudinal orientation in such a manner that the two cracks formed were either parallel or perpendicular to the fibre axis (Fig. 2). These crack lengths were designated C_z and C_x, respectively. The load was optimum in the sense that the cracks running perpendicular to the fibre axis were small enough so as not to interact with fibres. The crack length, $2c$, and indentor impression diagonal, $2a$, were measured for each indentation. Corresponding toughness values were then calculated for each set of two cracks formed by indentation (see Fig. 2). In the case of the transverse orientation, a set of indentations was made away from the row of fibres and another set near the row of fibres, as shown in Fig. 3. Again, the crack length and impression size were measured in the directions parallel, x, and perpendicular, y, to the row of fibres (see Fig. 3). Corresponding toughness values were designated x_{away}, x_{near}, y_{away}, and y_{near} (the subscripts near or away signifying whether the indentation was made near or away from the row of fibres). A set of 10 indentations was made for each type of sample. The fracture toughness of the matrix was calculated using the following equation [8]

$$\left(\frac{K_C\phi}{Ha^{1/2}}\right)\left(\frac{H}{E\phi}\right)^{0.4}(\alpha) = \left(\frac{c}{a}\right)^{(c/18a)-1.51} \quad (2)$$

where K_C is the mode I fracture toughness, H is the hardness of the matrix, a is half of the indentor impression diagonal, c is the crack length, E is the elastic modulus of the matrix, α is a non-dimensional constant, dependent on Poisson's ratio of the matrix, and ϕ is a constraint factor ≈ 3.0.

2.3. Critical load, P_C

Monolithic zircon and zircon matrix between the fibres in four types of composites were indented at

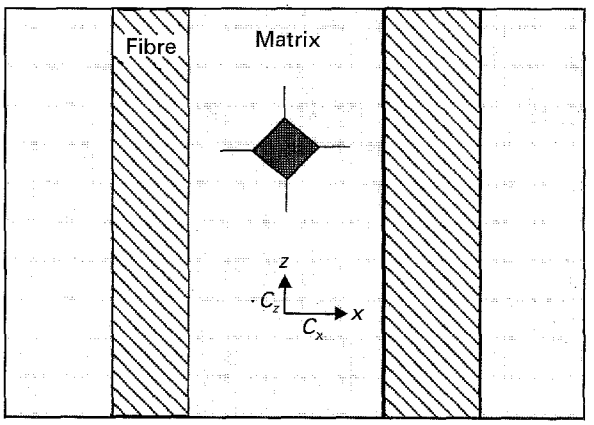

Figure 2 Schematic illustration of a composite polished in the longitudinal orientation. C_z and C_x refer, respectively, to cracks formed along and perpendicular to the fibre axis.

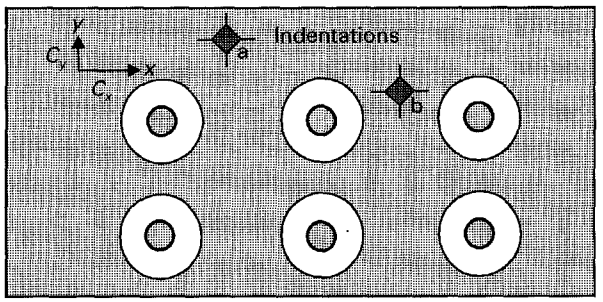

Figure 3 Cross-section of a composite polished in the transverse direction. C_x and C_y are cracks along the x and y directions, respectively.

different locations to determine the minimum load needed for crack initiation at the corners of the indentation impression. This was done in both the longitudinal and transverse orientations. Again, a set of 10 indentations was made for each orientation to determine the average value.

3. Results and discussion

3.1. Matrix properties

The hardness of the monolithic zircon, as determined by the Vickers indentation method, was 12.4 GPa. This was higher than any of the measured hardness numbers for the matrix within a composite. The fracture toughness was 1.9 MPa $m^{1/2}$, which is lower than the toughness values for the matrix in the composite samples. The critical load needed to initiate cracks in the monolithic zircon was 0.15 kg.

3.2. Residual stress state of the matrix in the composite

Residual stresses in the matrix are created by the thermal expansion mismatch between the fibre and the matrix. These residual stresses have been calculated earlier by various authors [24–28]. The thermal expansion coefficients of SCS-6 and SCS-0 fibres, and zircon matrix are 4.89×10^{-6}, 4.44×10^{-6}, and $5.17 \times 10^{-6}\,°C^{-1}$, respectively [29]. The difference in the coefficients of thermal expansion between the fibre and the matrix leads to residual stresses in the axial and radial directions in the composite. If the coefficient of thermal expansion of the matrix, α_m, is higher than the corresponding value for the fibre, α_f, then this causes axial tensile stresses in the matrix and radial compressive stresses at the fibre–matrix interface and in the matrix. Conversely, if $\alpha_f > \alpha_m$ then the matrix is under axial residual compressive stress and the fibre–matrix interface experiences a radial tensile force. As $\alpha_m > \alpha_f$ in the present system, this should give rise to a tensile stress, σ_z, in the axial direction, as shown in Fig. 4. The stress in the radial direction at the fibre–matrix interface is compressive due to the thermal expansion mismatch, but it can change to tensile stress away from the fibres. The explanation for the origin of this tensile stress is shown in Fig. 4. Fig. 4a

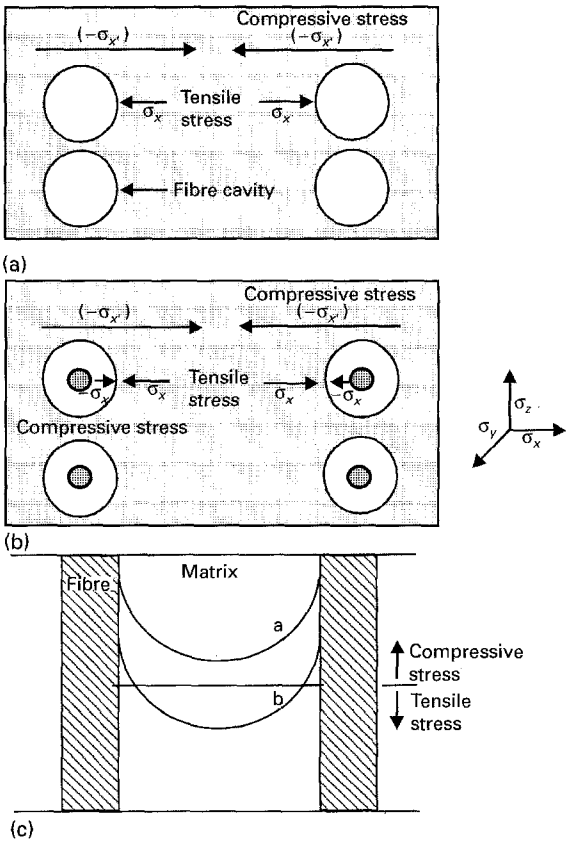

Figure 4 Schematic illustration of a composite showing the nature of residual stresses. Regions between two fibres may experience a tensile stress (minima in curve b) or a lower compressive stress (minima in curve a) between fibres. In contrast, areas near the fibre are under compressive stress.

illustrates a hypothetical situation where the fibres from the composite have been removed and, as a result, the matrix now has cavities in place of the fibres. The region of the matrix between any two fibre cavities experiences a tensile force because, on cooling, the matrix tries to contract in opposite direction into these cavities which contained the fibres. This results in a tensile stress, σ_x, in the matrix, as shown in Fig. 4a. Now, consider the next situation, as shown in Fig. 4b, where the fibres have been placed back into the cavities. In this case, the matrix is no longer able to contract into the cavities which are occupied by the fibres and hence, this results in a radial compressive force ($-\sigma_x$) at the fibre–matrix interface. The resulting stress state due to the tensile and compressive stresses as described in Fig. 4a and b is shown in Fig. 4c. Curve (a) represents a situation where the compressive stress is high near the fibres and decreases as the radial distance increases. Curve (b) represents another situation where the stress away from the fibres is tensile in nature, but it is still compressive when the radial distance is small. Either of the two cases is possible during processing and the final stress state will be a function of various parameters such as coefficients of thermal expansion, Poisson's ratios, and elastic moduli of the fibre and matrix. Also, the unreinforced areas of the matrix at the top and bottom of the composite have no fibres and hence a net compressive stress ($-\sigma'_x$) exists.

3.3. Dependence of matrix hardness on interfacial shear strength

A plot of the variation in hardness with a change in interfacial shear strength is shown in Fig. 5. It can be seen that the hardness values for samples in the transverse orientation are higher than the corresponding values in the longitudinal orientation. This can be explained by considering the stress state in the matrix, as discussed in the previous section. Lower hardness in the longitudinal orientation suggests that a tensile stress, σ_x, exists in the radial direction (Fig. 4c, curve b). This radial tensile stress, coupled with the additional tensile stress, σ_z, in the axial direction results in a lower hardness because these tensile stresses facilitate the penetration of the indentor into the matrix upon application of the load to the indentor. In the case of transverse orientation, only one of these stresses, σ_x, exists and hence the hardness is higher in comparison to that in the longitudinal orientation. It can also be seen that the hardness in the transverse orientation is, in general, higher for samples fabricated by using carbon-rich and silicon-rich fibres in comparison to those made from boron nitride-coated and uncoated fibres. This can again be explained by considering the effect of the radial compressive stress resulting from thermal expansion mismatch. The values of the radial compressive stress as found experimentally with the fibre push-out test [24] and theoretically calculated by the thick cylinder model, are given in Table II. In the case of C-R and Si-R samples, both the experimental and calculated values of the residual stresses are higher than the corresponding values for the BN and UNC samples. A higher radial compressive stress, combined with the tensile stress, σ_x, can result in a lower net tensile stress, or even a net compressive stress in the matrix. As a consequence, more resistance to penetration occurs during indentation and this results in a higher hardness value. These observations on hardness values suggest that the coefficient of thermal expansion of the matrix is higher than that of the fibre, which is in agreement with the earlier results of Reddy *et al.* [24].

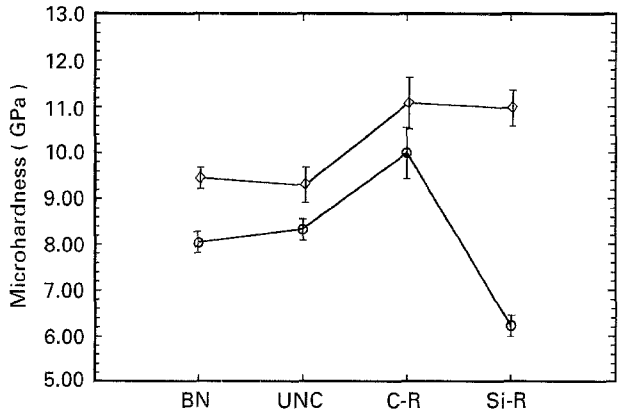

Figure 5 Dependence of matrix hardness on interfacial shear stress for samples in the (○) longitudinal (LN) and (◇) transverse (TR) orientations.

3.4. Dependence of fracture toughness on interfacial shear strength

3.4.1. Longitudinal orientation

Fig. 6 shows results for samples in the longitudinal orientation. A general trend of higher fracture toughness in the x direction is seen in comparison to data in the z direction. A consistent decrease in fracture toughness with increasing interfacial shear strength (from BN to C-R) is also observed. In addition, there seems to be a small increase in fracture toughness from sample C-R to Si-R. The dependence of fracture toughness on constituent material parameters can be assessed by using Equation 2. In this equation, the fracture toughness is directly related to $(c/a)^x$ (where $x = (c/18a) - 1.51$), $1/H^{0.4}$ and $a^{1/2}$. A comparison of Fig. 6 with Fig. 5 indicates that there is an inverse relationship between the fracture toughness and hardness. Also, a comparison of Fig. 6 with Fig. 7 shows a very high degree of inter-dependence between the fracture toughness and (c/a) ratio. Thus, we see that the parameter (c/a) has a much stronger influence on toughness and dominates over the effect of hardness on fracture toughness values. This influence of (c/a) ratio on fracture toughness can be used to explain the different fracture toughness values calculated by using the crack lengths in x and z directions, and also the variation in toughness with increasing interfacial shear strength. The magnitude of the (c/a) ratio can be affected by the presence of the axial and radial residual stresses in the matrix. Fig. 7 shows that the (c/a) values in the x direction are distinctly lower than the values in the z direction. Fig. 8a illustrates the effect of the residual stresses on the indentation crack lengths for

TABLE II Experimental and theoretical values of the residual radial and axial stresses in the matrix resulting from the thermal expansion mismatch between the fibre and the matrix [22]

Composite (coating)	Axial stress (MPa)		Radial stress (MPa)	
	Theoretical	Experimental	Theoretical	Experimental
BN (boron nitride)	− 36.1	–	39.8	31.67
UNC (uncoated)	− 36.1	− 57.8	39.8	31.63
C-R (carbon-rich)	− 109.1	− 48.7	95.7	14.88
Si-R (silicon-rich)	− 109.1	–	95.7	–

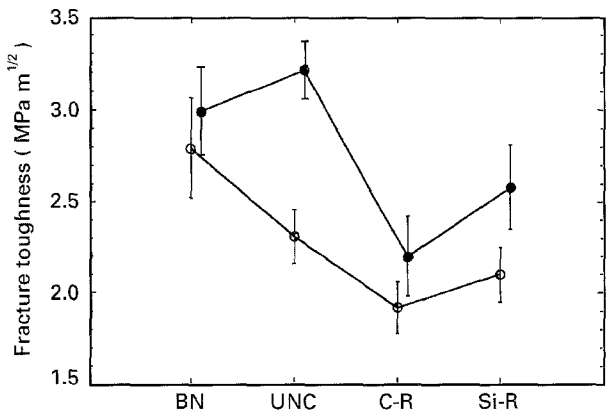

Figure 6 Fracture toughness values as a function of the interfacial shear strength for composites in the longitudinal orientation. (○) z, (●) x.

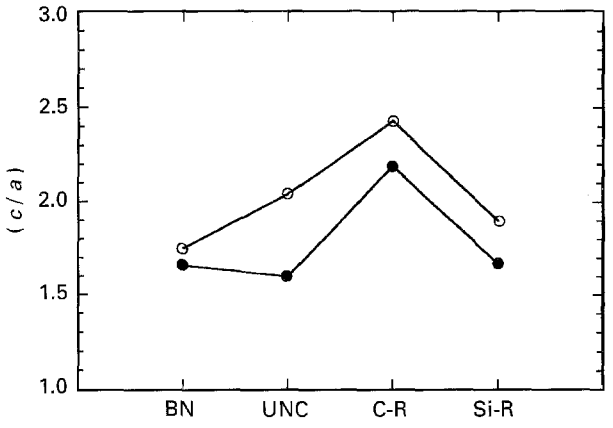

Figure 7 Influence of interfacial shear strength on the (c/a) ratio for the composites in the longitudinal orientation (see Section 2.2). (○) z, (●) x.

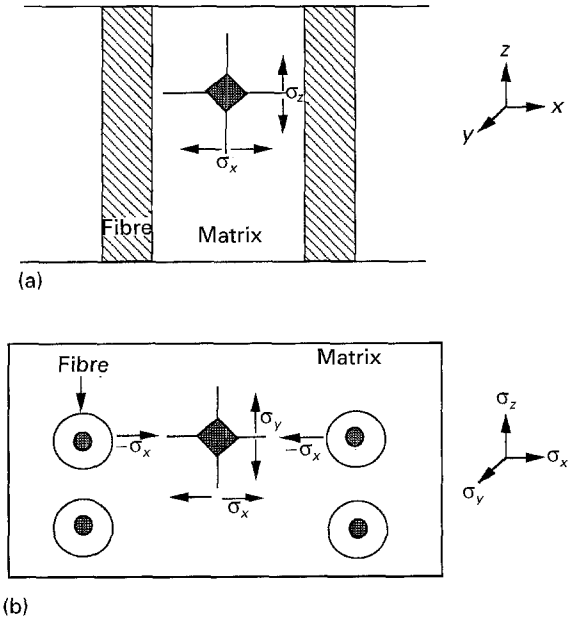

Figure 8 Schematic illustration of a composite showing the effect of axial and radial residual stresses on the indentation crack lengths. In longitudinal orientation (a), axial stress, σ_z, and radial stress, σ_x, influence the crack lengths in the x and z directions, respectively. In the transverse orientation (b), tensile stress, σ_x, increases the crack length in the y direction. Compressive stresses ($-\sigma_x$) near the fibres results in tensile stress, σ_y, on indentation and this increases the crack length in the x direction.

a sample in the longitudinal orientation. The axial-stress, σ_z, and the radial stress, σ_x, tend to increase the crack length in the x and z directions, respectively. The above observation of longer crack length in the z direction indicates that the radial stress, σ_x, is higher than the axial stress, σ_z. The fracture toughness values for composites BN and UNC are higher than for composites C-R and Si-R. This could be because of the lower value of the axial tensile stress, σ_z, as a result of the interfacial sliding at the weak interface. Also, the state of the radial stress, σ_x, may change due to interfacial sliding and this could, in turn, result in lower tensile residual stresses and higher fracture toughness values.

3.4.2. Transverse orientation

In the case of transverse orientation, the uncoated sample (UNC) has the highest toughness values in all cases, while C-R has the lowest values (Fig. 9). In the case of samples BN, C-R and Si-R, the fracture toughness values are lower, in general, for the cracks parallel to the row of fibres (i.e. x_{away} and x_{near}) in comparison to the cracks perpendicular to the row of fibres (i.e. y_{away} and y_{near}). Fig. 9 also reveals that the fracture toughness for cracks parallel to the row of fibres is higher for indentations made away (x_{away}) in comparison to those near the fibres (x_{near}), except in the case of C-R where a significant difference is not seen. These observations suggest a possible influence of fibres on crack growth in the matrix. Again, a comparison of Figs 9 and 10 shows that the parameter (c/a) has a strong influence on fracture toughness values for the transverse orientation, as was seen in the case of longitudinal orientation in Section 3.4.1. Therefore, a better appraisal of the influence of fibres on crack growth and fracture toughness is possible by studying the changes in the parameter (c/a) for samples having different interfacial shear strength values (Fig. 10). First observation from Fig. 10 is that the (c/a) ratio for the cracks in the x direction is greater in comparison to that for cracks in the y direction for composites. BN, C-R and Si-R. This suggests that the crack extension in the y direction faces a resistance because of the

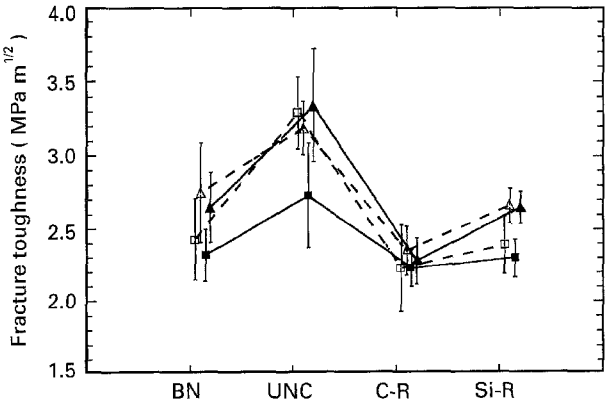

Figure 9 Fracture toughness for the samples in transverse orientation (– –□– –) x_{away}, (– – △ – –) y_{away}, (—■—) x_{near}, (—▲—) y_{near}.

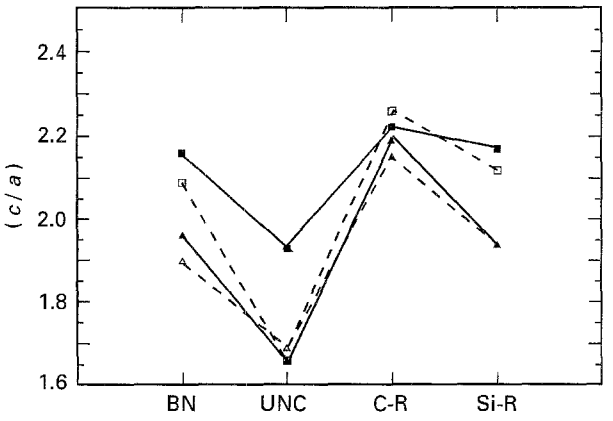

Figure 10 (c/a) ratio as a function of the interfacial shear strength for composites in the transverse orientation. (– -□- –) x_{away}, (– – △– –) y_{away}, (—■—) x_{near}, (—▲—) y_{near}.

compressive stress, resulting in the matrix area of the composite where there are no fibres, as shown in Fig. 4a. The second observation is the higher c/a values obtained when the indentations are made near the row of fibres in comparison to those made away from the fibres. This is true for cracks in both the x and y directions. In this case, the crack length in the y direction increases as the indentations are made near the fibres because the compressive force ($-\sigma'_x$) becomes lower in magnitude, and hence offers lower resistance to crack extension (Fig. 8b). However, the crack extension in the the x direction is restricted due to the presence of fibres near the indentation, which results in a compressive stress. Also, the presence of a compressive stress ($-\sigma_x$) in the radial direction near the fibres (Figure 8b) contributes to crack extension in the x direction. Thus, the matrix region in the vicinity of the crack tip experiences a tensile stress, σ_y, in the direction perpendicular to the radial compressive force, as shown in Fig. 8b. This tensile stress, coupled with the tensile stress that results because of the indentation load, creates a longer crack length when the indentations are made near the row of fibres. For samples having higher interfacial shear stress, the radial compressive stress increases and this should lead to lower crack length in the y directon and higher length in the x direction. Fig. 10 shows that the crack length in the x direction for indentatons near the fibres tends to increase with higher interfacial shear stress values, with the exception of sample UNC. For the cracks in the y direction, the variation in the crack lengths as a function of the interfacial shear stength is not clear. The inconsistent variation in the crack lengths in the transverse orientation can be explained by considering that only radial stress, σ_x, is present in this orientation, unlike in the longitudinal orientation where both radial *and* axial stresses influence the crack lengths. Also, the deviation in the position of the fibres from the regular square array (as assumed in Fig. 3) is expected to change the stress distribution within the matrix which is expected to affect the results.

3.5. Critical load measurements

A plot of the minimum indentor load, P_C, needed to initiate cracks at the corners of the Vickers indentation for the four types of sample is shown in Fig. 11. The critical load values for composites fabricated using uncoated and boron nitride-coated SCS–6 fibres are appreciably higher than those composites having carbon-rich and silicon-rich fibre surfaces. In addition, the P_C values in the longitudinal orientation for composites BN and UNC are higher than the corresponding values in the transverse orientation. A comparison of the critical load data in Fig. 11 with the average fracture toughness values in the longitudinal and transverse orientations indicates that the critical load scales with the fracture toughness values. The average toughness of sample BN is higher in the longitudinal orientation (2.9 MPa $m^{1/2}$) than in the transverse orientation (2.5 MPa $m^{1/2}$) (Table III). Accordingly, the critical load is higher in the longitudinal orientation (1.0 kg) in comparison with the transverse orientation (0.5 kg). For the sample containing uncoated fibres, a reverse trend is seen. Here, the fracture toughness is higher in the transverse orientation but a correspondingly higher critical load is not seen. In the case of C-R, the toughness values for the two orientations are very close to each other (2.1 MPa $m^{1/2}$ for the longitudinal and 2.3 MPa $m^{1/2}$ for the transverse orientation). Correspondingly, we see that the critical load values are equal (0.15 kg) for composite C-R in both orientations. In the case of a sample made from fibres having a silicon-rich surface, the average fracture toughness value is higher in the transverse orientation (2.5 MPa $m^{1/2}$) than in the longitudinal orientation (2.1 MPa $m^{1/2}$). When compared with the critical load data, it can be seen that the critical load is also slightly higher for the transverse orientation (0.15 kg) than the load required for the longitudinal orientation (0.12 kg). These results indicate that the critical load

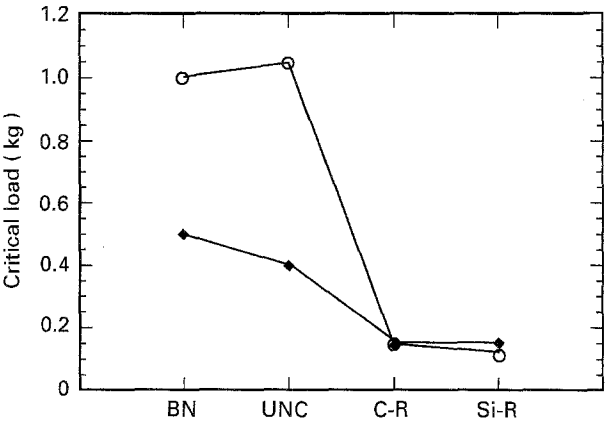

Figure 11 Dependence of the critical load needed to initiate cracks on the interfacial shear strength. (○) LN, (◆) TR.

TABLE III Average fracture toughness, K_C (MPa $m^{1/2}$), values in the longitudinal (LN) and transverse (TR) orientations

Composite type	K_C (LN)	K_C (TR)
BN	2.9 ± 0.25	2.5 ± 0.25
UNC	2.8 ± 0.50	3.1 ± 0.40
C-R	2.1 ± 0.23	2.3 ± 0.18
Si-R	2.1 ± 0.20	2.5 ± 0.20

can be directly related to the average fracture toughness value in the two orientations for these samples.

4. Conclusions

1. A micro-indentation technique using the Vickers micro-indentor was successfully used to study the matrix properties on a micro-scale in continuous fibre-reinforced ceramic composites.

2. Properties of the zircon matrix in fibre-reinforced composites were found to be different from the monolithic zircon. The fracture toughness of the monolithic zircon was lower (1.9 MPa $m^{1/2}$) and the hardness was higher (12.4 GPa) than the corresponding values of the zircon matrix in several composites. The critical load for the monolithic zircon was 0.15 kg, which was lower than the values for the matrix in the composite samples fabricated using uncoated and boron nitride-coated fibres. This value of the critical load was the same as that for samples made with fibres having carbon-rich and silicon-rich surfaces.

3. The matrix exhibits distinctly anisotropic behaviour in terms of the hardness and fracture toughness values. The observed anisotropy occurs because of the presence of radial and axial residual stresses in the composite. These residual stresses are created by the thermal expansion mismatch between the fibre and the matrix.

4. There exists a direct correlation between the fracture toughness and the critical load needed to initiate cracks in the matrix. A knowledge of the minimum load needed to initiate cracks in the matrix becomes important because this load signifies the onset of mechanical and chemical degradation of the composite.

Acknowledgements

We thank Dr Susmit Kumar for his comments on the manuscript. This project was supported by the US Department of Energy, Basic Energy Sciences Division under contract number DE-FG02-91ER45459.

References

1. A. G. EVANS, *Mater. Sci. Eng.* **A107** (1989) 227.
2. A. G. EVANS, F. W. ZOK and J. DAVIS, *Compos. Sci. Technol.* **42** (1991) 3.
3. R. J. KERANS, R. S. HAY, N. J. PAGANO and T. A. PARTHASARATHY, *Ceram. Bull.* **68** (1989) 429
4. J. LANKFORD, *J. Mater. Sci. Lett.* **1** (1982) 493.
5. K. NIHARA, *ibid.* **2** (1983) 221.
6. C. B. PONTON and R. D. RAWLINGS, *Mater. Sci. Technol.* **5** (1989) 961.
7. G. R. ANSTIS, P. CHANTIKUL, B. R. LAWN and D. B. MARSHALL, *J. Am. Ceram. Sco.* **64** (1981) 533.
8. K. M. LIANG, G. ORANGE and G. FANTOZZI, *J. Mater. Sci.* **25** (1990) 207.
9. A. G. EVANS, "Fracture Mechanics Applied to Brittle Materials", ASTM STP 678, edited by S. W. Freiman (American Society for Testing and Materials, Philadelphia, PA 1979) pp. 112–35.
10. Hj. MATZKE, *Key Eng. Mater.* **56-57** (1991) 365.
11. M. HIRANO and H. INADA, *J. Mater. Sci.* **27** (1992) 3511.
12. G. BABINI, A. BELLOSI and C. GALASSI, *ibid.* **22** (1987) 1687.
13. R. BERRICHE, R. T. HOLT, S. N. KUMAR and T. M. MACCAGNO, *Ceram. Eng. Sci. Proc.* **13** (1992) 966
14. A. K. MUKHOPADHYAY, S. K. DATTA and D. CHAKRABORTY, *Ceram. Int.* **17** (1991) 121.
15. D. K. SHETTY, I. G. WRIGHT, P. N. MINCER and A. H. CLAUER, *J. Mater. Sci.* **20** (1985) 1873.
16. T. HANSSON, R. WARREN and J. WASEN, *J. Am. Ceram. Soc.* **76** (1993) 841.
17. K. BREDER, K. ZENG and D. J. ROWCLIFFE, *Ceram. Eng. Sci. Proc.* **10** (1989) 1005.
18. P. F. BECHER and G. C. WEI, *Commun. Am. Ceram. Soc.* **67** (1984) C267.
19. J. WANG, M. R. PIRAMOON, C. B. PONTON and P. M. MARQUIS, *Br. Ceram. Trans.* **90**(4) (1991) 105.
20. K. L. POWELL, J. A. YEOMANS and P. A. SMITH, *ibid.* **92**(1) (1993) 23.
21. R. N. SINGH, *J. Mater. Sci.* **26** (1991) 1839.
22. S. K. REDDY and R. N. SINGH, "Ceramic Transactions", Vol. 38, "Advances in Ceramics-Matrix Composites", edited by N. P. Bansal (American Ceramic Society, Westerville, OH, 1993) pp. 211–22.
23. H. E. BOYER (ed.) "Hardness Testing", (ASM International, Metals Park, OH, 1990) Ch. 4.
24. B. BUDIANSKY, J. W. HUTCHINSON and A. G. EVANS, *J. Mech. Phys. Solids* **34** (1986) 167.
25. Y. MIKATA and M. TAYA, *J. Compos. Mater.* **19** (1985) 554.
26. M. KUNTZ, B. MEIER and G. GRATHWOHL, *J. Am. Ceram. Soc.* **76** (1993) 2607.
27. C. M WARWICK and T. W. CLYNE, *J. Mater. Sci.* **26** (1991) 3817.
28. J. X. LI, Y. MATSUO and S. KIMURA, *J. Ceram. Soc. Jpn* **100** (1992) 502.
29. S. K. REDDY, S. KUMAR and R. N. SINGH, *J. Am. Ceram. Soc.* **77** (1994) 3221.

Received 27 June 1994
and accepted 8 June 1995